Paper

Diagnostics and Investigations of the Plasma and Field Properties in Pulsed-Plasma Configurations

Konstantin Tsigutkin* Non-member
Eyal Kroupp* Non-member
Evgeny Stambulchik* Non-member
Dmitry Osin* Non-member
Rami Doron* Non-member
Ron Arad* Non-member
Alexander Starobinets* Non-member
Yitzhak Maron* Non-member
Ingo Uschmann** Non-member
Eckhart Förster** Non-member
Amnon Fisher*** Non-member

Spectroscopic methods recently developed for the measurements of electric fields, magnetic fields, and plasma properties in various pulsed-power systems are described. The methods utilize spectroscopy of visible-UV and X-ray emission-lines and of laser radiation. They allow for non-perturbing measurements with relatively high spectral, temporal, and spatial resolutions. Spatial resolution along the line of sight is obtained by locally doping the plasma with various species whose emission is then utilized. A few methods developed for doping solid and gaseous materials are described. Results for an ion diode, nanosecond and microsecond Plasma Switches, and a pinch system are presented.

Keywords: plasma spectroscopy, pulsed power, laser spectroscopy, X-ray spectroscopy, plasma switches, Z-pinches

1. Introduction

Spectroscopic methods are highly useful in achieving reliability and accuracy in investigations of numerous complicated pulsed-power systems. These methods can be applicable to a wide variety of devices, including electron diodes [1], ion diodes [2], high power magnetrons [3], plasma opening switches [4], and various plasma implosion devices such as Z-pinches [5]. Techniques recently developed allow for determining the electric field distribution from Stark shift [6] [7] and broadening [8]~[10], the magnetic field distribution from Zeeman splitting [11]~[15], the ion velocity distribution from Doppler broadenings and shifts [16]~[18], the electron temperature from line-intensity ratios [19], the electron density from the particle ionization times [17] [18], and the particle density distributions from the absolute intensities of various spectral lines [20]. Laser spectroscopy allows for particularly high-spatial-resolution measurements of ion velocities, electron density and temperature, and electric fields [21]. For analyzing the line intensities in such non-equilibrium plasma we use detailed time-dependent collisional-radiative calculations [22]~[25]. Measurements with high-spatial-resolution in three dimensions are crucial for obtaining unambiguous results. Such measurements are obtained by locally doping the plasma with various species and observing the characteristic emission of those species.

2. Anode-plasma properties in an ion diode

Here, the properties of the anode plasma within tens of μm from the anode surface were determined using laser absorption and laser-induced-fluorescence [21]. To this end, the anode surface was doped with magnesium that was released from the surface in the flashover process that produced the anode plasma. The laser beam was passed through the plasma, and the spectral profile of the laser light transmitted through the plasma was observed. An example of such a profile for the Mg II $3s - 3p\ ^2P_{3/2}$ transition is shown in Figure 1. The true line spectral profile, deconvolved from the measured spectral profile of the transmitted laser light using the spectral instrumental response, was used to obtain the

* Weizmann Institute of Science, Rehovot, Israel

** Firedrich-Shiller Univesität, Jena, Germany

*** Technion - Israeli Institute of Technology, Haifa, Israel

absorption coefficient $\alpha(\lambda)$. Gaussian curves were found to fit most of the data satisfactorily, giving the total absorption coefficients $\alpha(\lambda_0)$ at the line centers and the absorption line full widths (σ_{FWHM}) for the different species. In order to determine the density N_l of the lower level of the transition, we use the formula

$$N_l = \frac{\alpha(\lambda_0)\ \sigma_{FWHM}}{p_0 f_{lu} \lambda_0^2} + N_u \frac{g_l}{g_u},$$

where σ_{FWHM} is in Å, $p_0 = 8.3 \times 10^{-21} cm^2/$Å for a Gaussian and $5.65 \times 10^{-21} cm^2/$Å for a Lorentzian, f_{lu} is the absorption oscillator strength, λ_0 is the wavelength in Å at the line center, densities are in cm^{-3}, and $\alpha(\lambda_0)$ is in cm^{-1}. The measured densities as a function of distance from the anode surface of the Mg II ground (3s) and excited (3p $^2P_{3/2}$) states are shown in Figure 2. The data point closest to the surface is at $x = 15$ μm, since it represents an average over the 30-μm-wide region near the surface. It is obtained from the absorption of the laser light scattered on the anode surface.

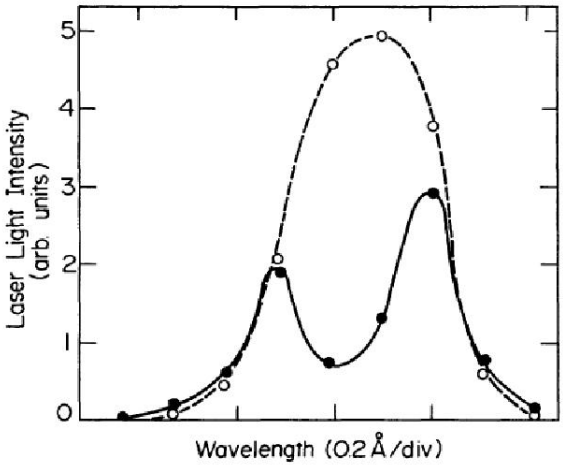

Fig. 1. A typical spectral profile of the laser light transmitted through the plasma (solid curve). The laser light wave length is $\lambda \approx 2795.5$ Å, the center of the Mg II $3s - 3p\ ^2P_{3/2}$ transition. The curves indicate the trend. The dip in the solid curve is due to resonant absorption of the laser light in the plasma (see text).

Using the collisional-radiative calculations for a wide range of electron temperatures and densities, we found that most of the Mg II ions lie in the 3s and 3p levels. The density gradients shown in Figure 2, reveal, therefore, a large gradient in the Mg II total density near the anode surface.

It is instructive to show the limitation of the use of spontaneous emission for measurements at such small distances from the surface. In Figure 2(b) the Mg II 3p $^2P_{3/2}$ level density is shown together with the observed emission intensity of the 3p $^2P_{3/2}$ – 3s transition as a function of distance from the surface. It is seen that the emission intensity observed decreases near the surface, thus failing to show the density rise there. Using ray-tracing calculations [26], we verified that this resulted from the effects of self-absorption, limited spatial resolution, and low light collection efficiency near the surface that affect the spontaneous-emission measurements.

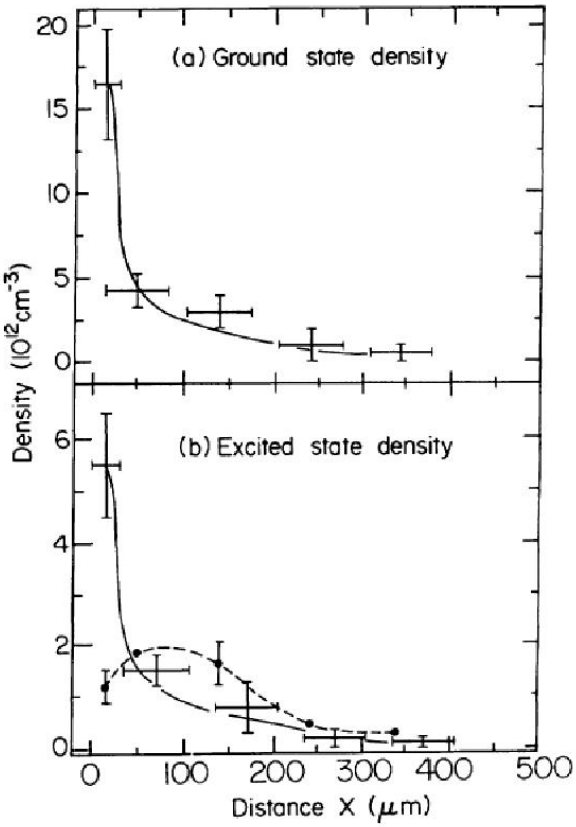

Fig. 2. (a) The Mg II ground-state density as a function of the distance x from the anode surface obtained from the laser absorption at 2795.5 Å for $t = 55$ ns. The spatial resolution near the anode surface is $\approx 30\mu$m. The curve indicates the trend. The data reveal a large density gradient of the Mg II ground state near the anode surface. (b) Similar to (a) for the density of the Mg II excited state $3p\ ^2P_{3/2}$ obtained from the laser absorption at 2798 Å (solid curve), and the intensity of the $3p\ ^2P_{3/2} - 3s$ emission in arbitrary units (dashed curve). The curves indicate the trends.

3. Doping techniques

In order to obtain spatial resolution along the line of sight the plasma is locally doped with various species whose emission is used for the various spectroscopic measurements. A variety of doping techniques have been developed. In all the doping techniques it is verified that the doped-material density is significantly less than the background plasma density to avoid perturbation of the plasma. For doping with solid material one needs to ablate material initially deposited on a solid surface. In the diode experiment, the epoxy used for the anode was mixed with a powder of the desired-species compound [21]. By doping only in limited portions of the dielectric anode, local measurements in three dimensions

could be obtained.

In the nanosecond POS experiment [13], a pulsed laser was used to evaporate material, initially deposited on the anode surface, into the POS region. The laser pulse was applied at an appropriate time prior to the operation of the POS, producing a conical column between the POS electrodes with a diameter that increased from ≈ 0.2 cm near the anode to ≈ 1 cm in the middle of the POS gap (1.25 cm from the anode). The axial location of the doped column was varied by moving the laser spot on the anode strip.

In microsecond POS experiment [27], a secondary surface discharge between two electrodes, placed on epoxy resin that contains the desired dopant, was used to inject various species into the switch plasma. This flashover plate was positioned outside the highly transparent cathode and formed a column of plasma that expanded at typical velocities of $(2-5)\times 10^6$ cm/s, and the time delay was adjusted accordingly. The width of this column was found to increase from 1.2 cm near the cathode to 3-4 cm near the anode.

In order to dope gaseous materials, such as helium and other noble gases, another method using injection of a gas beam into the plasma was developed [28]. This system is currently being used to study the operation of the microsecond POS. The doping arrangement consists of a fast gas valve and a 0.8-mm-diameter nozzle. The valve is driven by a 2 μF, 6 kV capacitor, discharged through a low inductance strip-line. A skimmer is placed approximately 5 cm from the nozzle to further collimate the gas beam before it enters the POS region through the highly transparent cathode. Skimmers with apertures in the range 0.3-0.7-cm-in-diameter are used giving gas beams with FWHM that could be varied in the experiments from 0.7 to 1.6 cm.

4. Electric field measurements

Our E-field diagnostic method is based on LIF combined with line-shape analysis of dipole-forbidden transitions [10] [29]~[31]. The diagnostics makes use of the Li I 2p-4d (dipole-allowed) and the 2p-4f (dipole-forbidden) transitions. The experiments were performed in ns-POS configuration [13]. The ns-POS, shown in Figure 3, is coaxial. It is driven by a 4 kJ, 600 kV, 1.5 Ω LC-water-line pulse generator that produces a 300 kV pulse with quarter period of 100 ns. The plasma ($n_e = 2\times 10^{14}$ cm^{-3}) is produced by flashboard and is injected into the POS region through the anode. The emitted light is imaged by lenses onto the spectrometers.

The lithium doping beam is produced by the laser evaporation method. The dye laser is tuned to excite the LiI 4p level from the ground state (see Figure 4). Collisional excitations and de-excitations by the plasma electrons lead to a rise in the populations of the 4d and 4f levels (and other neighboring levels) as shown by the time-dependent collisional-radiative calculations.

The rise of the 3d level population, for example, allows for measuring reliably the 2p–3d profile, which is used to determine the lithium velocity distribution, see below. Furthermore, because of the small energy separation between the 4d and 4f levels, the 4d–4f collisional excitation and de-excitation, for the plasma parameters used in this experiment, dominate other processes that may affect the 4d and 4f level populations. Collisional-radiative calculations thus show that the populations of these two levels (divided by the respective degeneracies) are equal to within 4%, which is important for proper interpretation of the relative line intensities. Since the forbidden line amplitude strongly depends on the electric field strength [29], the forbidden line intensity is a reliable measure of the electric fields in the plasma. However, the determination of the forbidden-line intensity requires correct line-shape calculations for both the allowed and forbidden transitions.

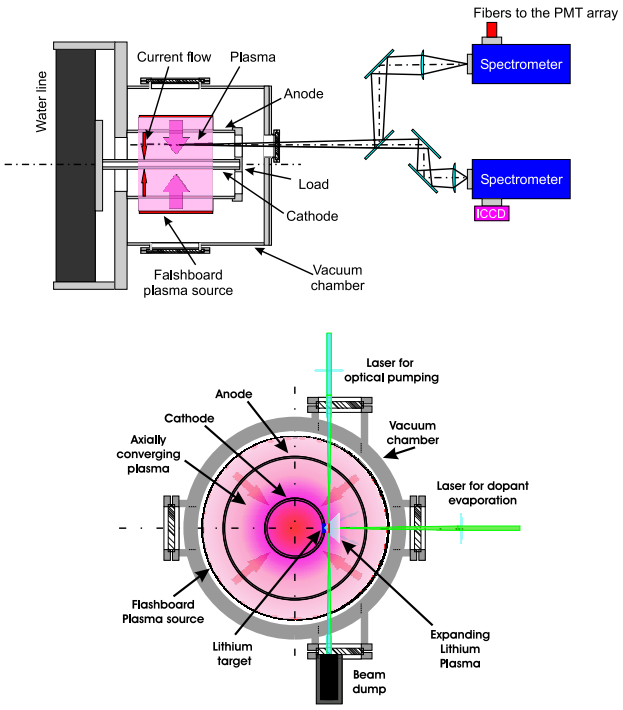

Fig. 3. Arrangement of the ns-POS and its diagnostic system.

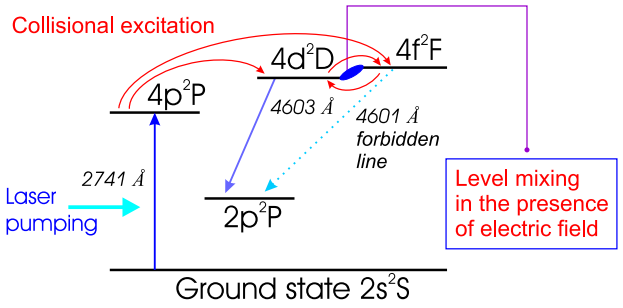

Fig. 4. A diagram of the laser-driven excitation of the Li I levels.

Here we describe measurements during the application of the generator current. We use the forbidden to allowed line ratios for determining the E-field in the plasma in the vicinity of the cathode surface (within 1 mm) during the current conduction. Figure 5 presents

the evolution of the electric field determined from the line ratios, where the current driven through the plasma starts at t = 0 ns. Also shown in Figure 5 are the upstream and downstream currents. It is seen in Figure 5 that the E-field prior to the rise of the generator current is ≈ 6 kV/cm, which is consistent with the 4d–4f mixing that results from the microfields in the 2×10^{14} cm^{-3} density flashboard plasma. During the current conduction the E-field rises and reaches its peak value, with an average of 12 kV/cm, at ≈ 55 ns, when the entire generator current is still conducted by the plasma (very small fraction of the current flows to the load).

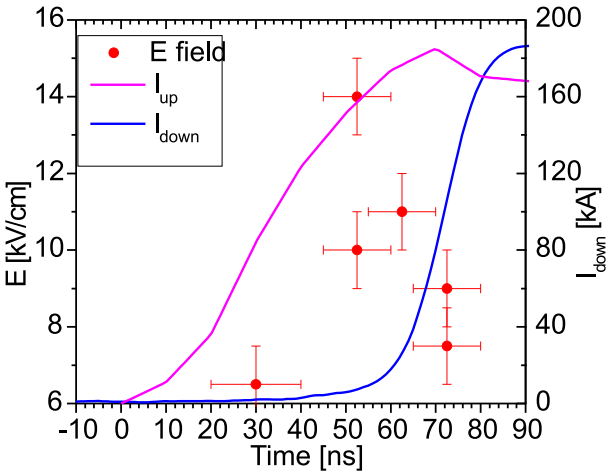

Fig. 5. E-field evolution during the current conduction. Here, $t = 0$ is the beginning of the generator current pulse. Also shown is the upstream and downstream currents(the current to the load) measured by Rogowsky coils.

The reason for the rise of the E-field requires further investigation. The field could rise due to a local rise in the plasma density, for example, due to plasma pushing by the magnetic field upstream of the measurement position. It can also be explained by a rise of electric fields in the plasma due to the current conduction. If this field is associated with the Hall potential in the plasma, it can then be estimated from the term $B^2/8\pi n_e e$, where B is the value of the self magnetic field at the location of the measurement and n_e is the local electron density. Using the typical values in our experiment for B (1 Tesla) and for n_e (2×10^{14} cm^{-3}), one obtains a value of 12 kV. For such a potential to produce $E \approx 6$ kV/cm, it must drop over a couple of cm (which should then be the current-channel width).

5. Magnetic field measurements using Zeeman splitting

The experiments were performed in microsecond planar POS configuration [27]. It consists of two planar, 14-cm-wide electrodes separated by a 2.5-cm gap. The current generator delivers a current of 200 kA during 400 ns, to be driven through a plasma prefilling the gap between two planar electrodes. The plasma density in the experiments is $\geq 10^{14}$ cm^{-3}. The basic diagnostic tool employed in this research is visible and UV spectroscopy. The evolution of the magnetic field is determined from the Zeeman splitting of the He I spectral line. The plasma was doped with helium and the 3d(^1D)–2p($^1P^0$) transition was observed. By observing emission from a neutral atom the Doppler broadening was minimized (unlike ions that are accelerated under the magnetic field gradient). Neutral helium has the unique feature that due to its slow ionization it can be used for this measurement throughout the entire experiment. Stark broadening is negligible for the electron density of 5×10^{14} cm^{-3} present in this experimental setup and the line width of the observed 6678 Å spectral line without the Zeeman splitting is thus dominated by the instrumental broadening.

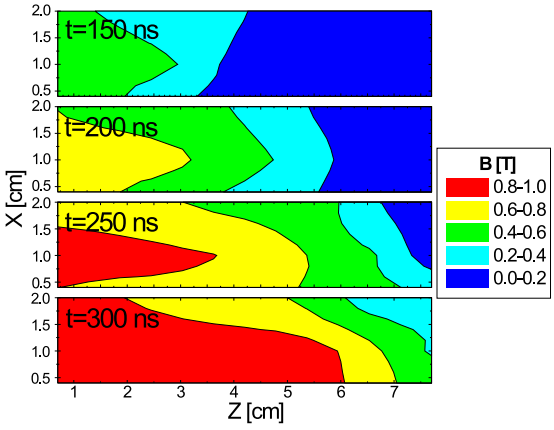

Fig. 6. Two-dimensional maps of the magnetic field (in Tesla) at four different times during the POS operation.

Figure 6 shows 2D maps of the magnetic field at t = 150, 200, 250, and 300 ns. The front of the magnetic field propagates at a velocity of 5×10^7 cm/s, while the value of B = 0.6 T propagates at a lower velocity of $(3.3 \pm 0.3) \times 10^7$ cm/s. At t = 150 and 200 ns the front of the magnetic field ($B \leq 4$ kG) is seen to propagate nearly in a 1-D form. At later times, however, the magnetic field structure for $B > 4$ kG resembles a wedge shape. In this figure at $x = 1$ cm, the width of the current-carrying region is seen to be 2–3 cm throughout the pulse, except near the anode at $t > 240$ ns, where it is even wider. At t = 300 ns a region with a low current density is formed at the generator-side edge of the plasma (near the cathode this region extends axially over most of the plasma). The reason for the lack of current flow at this position is probably related to the drop of the electron density in this region.

Comparison between the measured magnetic field distribution and the ion velocities, together with the analysis of the evolution of the electron density, is being presently used for improving our understanding of the magnetic field penetration into the plasma.

6. Ion velocity measurements in a Z-pinch plasma

Here we report on a time-resolved determination of the ion kinetic energy in a stagnating plasma in a gas-puff neon Z-pinch experiment. Measurements of the kinetic energy, performed in different experiments for different times throughout the entire X-ray emission period, allow for tracking the history of the ion kinetic energy. For these measurements we selected lines (Ly_α satellites) that, using radiation transport calculations, were verified to be free of opacity effects and, using Stark broadening calculations, were found to be insignificantly affected by Stark broadening. Also, we developed spectroscopic systems that provide rather high spectral resolution ($\lambda/\Delta\lambda \approx 6700$), which is evidently essential for such measurements. Furthermore, the spectroscopic systems employed allow for a simultaneous imaging the pinch column along its z axis, which provided information that is highly important for the data analysis. The data demonstrate that the ions lose most of their kinetic energy, reaching an energy comparable to the electron temperature, during the X-ray emission period. The gas in the present experiments is injected by two nozzles on the cathode side, where one is annular with a diameter of 38 mm delivering a gas load of ≈ 18 μg/cm, and the other is on axis, delivering ≈ 4 μg/cm. The implosion time is ≈ 750 ns, and the current at stagnation is ≈ 320 kA.

The main features of the spectroscopic systems developed for this study are the high spectral resolution ($\lambda/\Delta\lambda \approx 6700$) and the spatial imaging of the spectra with a resolution down to 0.1 mm. Single-gated MCP detectors followed by CCD cameras, provide 2-ns temporal resolution throughout the 20-ns X-ray emission period.

The crystal used for this study is a spherically curved KAP operated at the second order. Using double-grating measurements it was verified that the spectrograph-system spectral resolution is only limited by the crystal rocking curve. Employing a high-dispersion for the spectrograph (R = 612 mm) allowed for resolving the crystal rocking curve at the detector plane, giving a resolving power ≈ 6700 (i.e., the Lorentzian spectral response is 1.8 mÅ wide) and providing a spectral window of 60–100 mÅ. We also note that possible instrumental broadening due to the pinch size was shown to be negligible in the present measurements.

In order to measure the Doppler profiles in the stagnation phase, the crystal was designed to focus on three Ne Ly_α satellites (12.310 – 12.355 Å). In addition, a pinhole-photography system was used to provide filtered 2-D images of the pinch column at four gated times (≥ 1 ns delay between each gate). The other diagnostic tools included X-ray diodes (XRD) and a system of Ross filters [32], equipped with fast PIN-diode detectors.

The satellites observed in this study are [33] [34]: $2p^2\ ^1D_2 - 1s2p\ ^1P_1$, $2s2p\ ^3P_{0,1,2} - 1s2s\ ^3S_1$, and $2p^2\ ^3P_{0,1,2} - 1s2p\ ^3P_{0,1,2}$ where one is a singlet transition (12.355 Å) and the other two are triplet transitions with three components (between 12.305 to 12.310 Å) and six components (between 12.321 to 12.326 Å), respectively. Due to its relatively simpler spectral profile, the satellite most useful for the ion-velocity measurements is the singlet one. For our plasma parameters, the natural (Lorentzian) broadening of this line is mainly determined by the rates of the upper-level autoionization (3.7×10^{14} s^{-1}) and the radiative-decay (1.2×10^{13} s^{-1}), giving a natural width of 3.3 mÅ. This width, together with the instrumental spectral response (1.8 mÅ), determine the spectral resolution for these observations.

Employing the z-imaging described above for these Ly_α satellites revealed that they are first emitted from the region $z = 9-12$ mm, where $z = 0$ and $z = 14.4$ mm are the cathode and anode positions, respectively. We now discuss the measurements for this region.

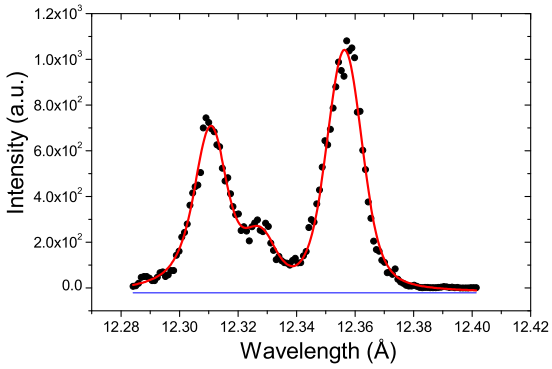

Fig. 7. Satellite spectrum for $z = 10.5$ mm, integrated over $\Delta z = 1.6$ mm, for $t = -3$ ns.

Figure 7 shows an example of the satellite structure observed at a relatively early time of the X-ray emission period, $t = -3$ ns, where $t = 0$ denotes the peak time of the XRD detector that collects > 800 eV photons from the entire pinch column. The resulting satellite profiles at $z = 10.5$ mm, and integrated over $\Delta z = 1.6$ mm, are shown in Figure 7. In order to obtain the Doppler contribution to the line width we assume a Gaussian shape for this contribution, where the other contributions are due to the Lorentzian natural broadening and instrumental response.

We thus fit Voigt profiles to each of the satellite components, where the Gaussian part is a parameter determined by the best fit. For the early time of the stagnation, the data give that the width (FWHM) of the Gaussian contribution to the profiles of the singlet satellite is between 8 and 11 mÅ(significantly larger than the natural width and the instrumental response width). The widths observed can only be associated with the Doppler effect, resulting from the ion thermal and hydrodynamic velocities. Indeed, assuming that each component of the other triplet satellites observed has the same width as the singlet satellite (consistent with Doppler-dominated widths), it was possible to reconstruct reasonably well

the satellite structure of the triplet satellites, as shown in Figure 7.

For later times the line emission was seen from the z region between $z = 6$ and 14.4 mm. Here, we only discuss the late emission from the region $z = 9 - 12$ mm, thus only addressing the time dependence of the ion kinetic energies at this region. An example of a satellite structure observed later in the stagnation is shown in Figure 8. It is seen that the Gaussian FWHM at $t = 6$ ns is 2.5 ± 0.6 mÅ. The Doppler contribution in this example corresponds to an ion temperature of 140 ± 75 eV. This is perhaps the lowest ion temperature expected to be detected since very plausibly the ions cannot be much colder than the electrons. Indeed, at this period of the stagnation the electron temperature is < 200 eV (which will be discussed elsewhere), demonstrating that the mean ion kinetic energy is tracked in our experiments down to T_e.

The measurements give the total kinetic energy of the H-like ions throughout the Ly_α-emission period ($t \approx -4$ to $t \approx +6$ ns relative to the XRD-signal peak).

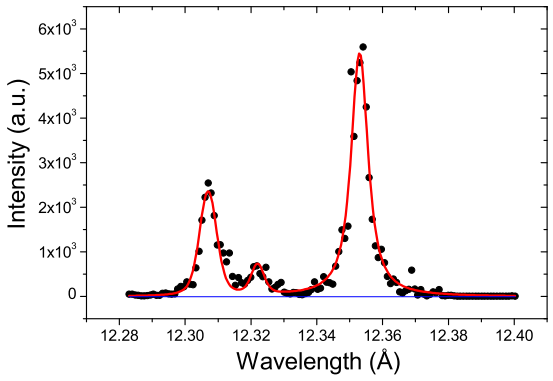

Fig. 8. Satellite spectrum observed at $z = 10$ mm and integrated over $\Delta z = 0.2$ mm, for $t = 6$ ns. The best-fit-Gaussian FWHM is 2.5 ± 0.6 mÅ.

7. Conclusions

Recent novel developments in spectroscopic diagnostics of pulsed-power systems allows a reasonable progress in obtaining very high-resolution measurements of the electric fields, magnetic fields, and plasma properties in a variety of pulsed-power systems utilizing a line and continuum emission from the plasma in the visible to the X-ray regions. Using doping techniques measurements spatially resolved in 3D are achieved. The use of laser absorption, laser-induced-fluorescence, and laser-enhanced emission of forbidden lines further improve the spatial resolutions and allow for the detection of relatively low electric field. Examples shown in this report are the determination of the properties of plasmas near surfaces in electrical discharges using laser spectroscopy, the electric fields in plasma using forbidden-line transitions, the magnetic field distributions from Zeeman splitting, the ion flow from the line-Doppler shifts, and electron temperature from line intensities. All information is obtained as a function of time and space. The measurements utilize various atomic-physics modeling, including collisional-radiative, line-broadening, and radiation-transport calculations. We believe that such or similar diagnostics can be applied beneficially to numerous electrical discharges or pulsed-power-transmission systems with various properties of the plasmas and of the fields.

Acknowledgment

This work was supported by the German-Israeli Project Cooperation Foundation (DIP), by the Minerva Foundation (Germany), and by the Israel Science Foundation.

(Manuscript received September 30, 2003, revised October 23, 2003)

References

(1) See, for example, R.B. Miller: "Intense Charged Particle Beams", Plenum, New York (1982), and references therein

(2) P. Dreike, C. Eichenberger, S. Humphries, and R.N. Sudan: "Production of intense proton fluxes in a magnetically insulated diode", *J. Appl. Phys.* **47**, 85 (1976); S. Humphries: *J. Nucl. Fusion* **20**, 1549 (1980); J.P. VanDevender: "Inertial confinement fusion with light-on beams", *Plasma Phys. Controlled Fusion* **28**, 841 (1986)

(3) T.J. Orzechowski and G. Bekefi: "Current flow in a high-voltage diode subjected to a crossed magnetic field", *Phys. Fluids* **19**, 43 (1976); "Microwave emission from pulsed, relativistic e-beam diods. I. The smooth-bore magnetron", **22**, 978 (1979)

(4) C. W. Mendel, Jr. and S. A. Goldstei: "A fast-opening switch for use in REB diode experiments", *J. Appl. Phys.* **48**, 1004 (1977); P. Ottinger, S.A. Goldstein, and R.A. Meger: "Theoretical modeling of the plasma erosion opening switch for inductive storage applications", *J. Appl. Phys.* **56**, 774 (1984)

(5) N.R. Pereira and J. Davis: "X rays from z-pinches on relativistic electron-beam generators", *J. Appl. Phys.* **64**, R1 (1988)

(6) Y. Maron, M.D. Coleman, D.A. Hammer and H.S. Peng: "Experimental determination of the electric field and charge distribution in magnetically insulated ion diodes", *Phys. Rev. A* **36**, 2818 (1987)

(7) J. Bailey, A.B. Filuk, A.L. Carlson, D.J. Johnson, P. Lake, E.J. McGuire, T.A. Mehlhorn, T.D. Pointon, T.J. Renk, W.A. Stygar, and Y. Maron: "Measurements of Acceleration Gap Dynamics in a 20-TW Applied-Magneric-Field Ion Diode", *Phys. Rev. Lett.* **74**, 1771 (1995)

(8) E. Sarid, Y. Maron, and L. Troyanski: "Spectroscopic investigation of fluctuating anisotropic electric fields in a high-power-diode plasma", *Phys. Rev. E* **48**, 1364 (1993)

(9) S. Alexiou, A. Weingarten, Y. Maron, M. Sarfaty, and Ya.E. Krasik: "Novel spectroscopic method for analysis of non-thermal electric fields in plasmas", *Phys. Rev. Lett.* **75**, 3126 (1995)

(10) E. Stambulchik: "Calculations of Spectral Line Broadening in Plasma", Ph.D. thesis, Weizmann Institute of Science (2002)

(11) Y. Maron, E. Sarid, E. Nahshoni, and O. Zahavi: "Time-dependent spectroscopic observation of the magnetic field in a high-power-diode plasma", *Phys. Rev. A* **39**, 5856 (1989)

(12) M. Sarfaty, R. Shpitalnik, R. Arad, A. Weingarten, Ya.E. Krasik, A. Fruchtman, and Y. Maron: "Spectroscopic Investigation of Fast (ns) Magnetic Field Penetration in a Plasma.", *Phys. Plasmas* **2(6)**, 2583 (1995)

(13) R. Shpitalnik, A. Weingarten, K. Gomberoff, Ya. Krasik, and Y. Maron: "Observation of two-dimensional magnetic field evolution in a Plasma Opening Switch", *Phys. of Plasmas* **5(3)**, 792 (1998)

(14) R. Arad, K. Tsigutkin, N. Chakrabarti, A. Fruchtman, and Y. Maron: "Spectroscopic investigations of the magnetic field

evolution and plasma flow in a microsecond POS", Proc. of the 12th Int. Conf. Beams 98 Haifa, Israel 253 (1998)
(15) G. Davara, L. Gregorian E. Kroupp, and Y. Maron: "Spectroscopic Determination of the Magnetic Field Distribution in an Imploding Plasma", *Phys. Plasmas* **5**, 1068 (1998)
(16) Y. Maron, E. Sarid, O. Zahavi, L. Perelumutter and M. Sarfaty: "Particle-velocity distribution and expansion of a surface-flashover plasma in the presence of magnetic fields", *Phys. Rev. A* **39**, 5842 (1989)
(17) M.E. Foord, Y. Maron, G. Davara, L. Gregorian, and A. Fisher: "Particle Velocity Distributions and Ionization Processes in a gas-puff Z pinch", *Phys. Rev. Lett.* **72**, 3827 (1994)
(18) M. Sarfaty, Y. Maron, Ya. E. Krasik, A. Weingarten, R. Arad, R. Shpitalnik, A. Fruchtman: "Spectroscopic Investigations of the Plasma Behavior in a Plasma Opening Switch Experiment", *Phys. Plasmas* **2(6)**, 2122 (1995)
(19) Y. Maron, M. Sarfaty, L. Perelmutter, O. Zahavi, M.E. Foord and E. Sarid: "Electron temperature and heating processes in a dynamic plasma of a high-power diode", *Phys. Rev. A* **40**, 3240 (1989)
(20) Y. Maron, L. Perelmutter, E. Sarid, M.E. Foord, and M. Sarfaty: "Spectroscopic determination of particle fluxes and charge-state distributions in a pulsed-diode plasma", *Phys. Rev. A* **41**, 1074 (1990)
(21) L. Perelmutter, G. Davara, and Y. Maron: "Plasma properties near the anode surface of an ion diode determined by high-resolution laser spectroscopy", *Phys. Rev. E* **50**, 3984 (1994)
(22) M.E. Foord, Y. Maron, and E. Sarid: "Time-dependent collisional-radiative model for quantitative study of nonequilibrium plasma", *J. Appl. Phys.* **68**, 5016 (1990)
(23) Yu.V. Ralchenko and Y. Maron: "Accelerated recombination due to resonant deexcitation of metastable states", *J. Quant. Spectr. Rad. Transfer* **71**, 609 (2001)
(24) R. Arad, K. Tsigutkin, Yu.V. Ralchenko, and Y. Maron: "Spectroscopic investigations of a dielectric-surface-discharge plasma source", *Phys. Plasmas* **7**, 3797 (2000)
(25) V. Fisher and Y. Maron: "Radiation effects on plasma kinetics", WIS preprint number WIS/22/03-SEPT-DPP (2003)
(26) L. Perelmutter, G. Davara, and Y. Maron: "Investigation of plasmas formed over dielectric surfaces using laser spectroscopy", Bull. Am. Phys. Soc. **35**, 2120 (1990)
(27) R. Arad, K. Tsigutkin, A. Fruchtman, J. D. Huba, and Y. Maron: "Observation of faster-than-diffusion magnetic field penetration into a plasma", *Phys. Plasmas* 10, 112 (2003)
(28) R. Arad, L. Ding, and Y. Maron: "Novel gas-doping technique for local spectroscopic measurements in pulsed-power systems", *Rev. Sci. Instr.* **69**, 1529 (1998)
(29) E. Stambulchik, K. Tsigutkin, and Y. Maron: "Recent Advances in Stark Line Broadening Calculations and their Applications to Precise Spectroscopy of Pulsed Plasmas", Proc. EPS-2003 Conf. St. Petersburg, July 2003
(30) M. Baranger and B. Mozer: "Light as a plasma probe", *Phys. Rev.* **123(1)**, 25 (1961)
(31) U. Rebhan, N.J. Wiegart and H.-J. Kunze: "Measurements of fluctuating electric fields by means of high-frequency Stark effect in a laser excited lithium beam", *Phys. Lett.* **85**, 228 (1981)
(32) E. Kroupp, A. Starobinets, E. Klodzh, Yu. V. Ralchenko, Y. Maron, I. N. Bogatu, and A. Fisher: "Investigation of Ne IX and Ne X line emission from dense plasma using Ross-filter systems", *J. Appl. Phys.* **92**, 4947 (2002)
(33) L.A. Vainshtein and U.I. Safronova: "Wavelengths and Transition Probabilities of Satellites to Resonance Lines of H- and He-like Ions", ADNDT **21**, 49 (1978)
(34) J.F. Seely: "Dielectronic Satellite Spectra to Lyman-Alpha", ADNDT **26**, 138 (1981)

Konstantin Tsigutkin (Non-member) was born in Novosibirsk, Russia in 1969. He received the M.Sc. Degree in physics from Novosibirsk University in 1992. Currently he completes writing the doctoral dissertation in the Physics Faculty at the Weizmann Institute of Science, Rehovot, Israel. His research interests include plasma-magnetic field interaction and plasma diagnostics using laser-induced fluorescence.

Eyal Kroupp (Non-member) is a Ph.D. student in the Plasma Laboratory at the Weizmann Institute of Science, Rehovot, Israel. From 1994 to 1997 he studied the implosion of a Z-pinch plasma, using high-resolution spectroscopic systems in the visible-UV spectrum, as a part of the M.Sc. degree. Since 1997 he studies the stagnation phase of the Z-pinch plasma in the soft X-ray spectrum, using high-resolution Bragg spectroscopy, employing cylindrical and doubly-curved crystals, Ross filters and pinhole systems, combined with fast (ns) MCP detectors.

Evgeny Stambulchik (Non-member) was born in Sverdlovsk, Russia in 1967. He received the Ph.D. degree in physics from the Weizmann Institute of Science, Rehovot, Israel, in 2002. His research interests cover spectral line broadening in plasmas, combined Stark and Zeeman effects, and polarization spectroscopy. Currently, he has a postdoctoral fellowship from the Weizmann Institute.

Dmitry Osin (Non-member) was born in Kharkov, Ukraine in 1976. He received the M.Sc. degree in physics from Kharkov State University. His research interests include the investigation of plasma dynamics under intense pulsed magnetic fields and high temporal and spatial resolution spectroscopy. Currently he is a Ph.D. student in the Physics Faculty at the Weizmann Institute of Science, Rehovot, Israel.

Rami Doron (Non-member) was born in Jerusalem, Israel in 1966. He received the Ph.D. degree in physics from the Hebrew University, Jerusalem, Israel in 2000. From 2000 to 2003 he worked on atomic physics research relevant to solar and astrophysics. His research interests include experimental and theoretical spectroscopy, autoionization and dielectronic recombination processes, solar physics, and X-ray astrophysics. Currently, he has a postdoctoral fellowship from the Weizmann Institute of Science, Rehovot, Israel, where he is working on pulsed power systems at the Plasma Laboratory.

Ron Arad (Non-member) was born in Amsterdam, Holland, on June 2, 1965. He received the Ph.D. degree in physics from Weizmann Institute of Science, Israel, in 2002, and works presently at the Soreq Nuclear Center, Yavne, Israel. He investigates interaction between magnetic field and plasma using high-resolution spectroscopic techniques.

Alexander Starobinets (Non-member) was born in Tomsk, Russia, on February 24, 1950. He received the Ph.D. degree in physics from the High Current Electronics Institute of the Academy of Science of the USSR in 1981, and is presently a Staff Scientist at Weizmann Institute of Science, Israel. He researches processes in nonequilibrium plasmas subjected to high energy deposition and models atomic physics processes for spectroscopic investigation of plasma.

Yitzhak Maron (Non-member) received the physics degree from the Weizmann Institute of Science, Rehovot, Israel in 1977. From 1980 to 1984, he worked on ion diodes at the laboratory of Plasma Studies at Cornell University, Ithaca, NY. Since 1988, he has been a Professor of Physics and the Head of the Plasma Laboratory at the Faculty of Physics, Weizmann Institute of Science. This laboratory specializes in the use of spectroscopy in the diagnostics of pulsed power systems and in developing theoretical models required for the data analysis and interpretation.

Ingo Uschmann (Non-member) received the physics degree from the Friedrich-Schiller-University, Jena, Germany in 1991. From 1992 to 1997 he was working at the Max Planck Society. From 1997 he worked as a Research Associate at Jena university. He had worked in X-ray optics, X-ray diffraction properties of bent crystals and ultrafast studies of solid matter by using time-resolved X-ray diffraction.

Eckhart Förster (Non-member) received in 1971 the Ph.D. and in 1985 the Habilitation from the Friedrich-Schiller-University, Jena, Germany. From 1971 to 1992 he was a Research Associate and Lecturer at the Friedrich Schiller University. Then he became head of the X-ray Optics Group of the Max Planck Society at the FSU, and later the head of the X-ray Optics Group of the Institute of Optics and Quantum Electronics at FSU. He had worked on X-ray diagnostics of laser produced plasmas by Bragg reflection on bent crystals.

Amnon Fisher (Non-member) received his Ph.D. degree in physics from the Weizmann Institute of Science, Rehovot, Israel in 1972. From 1974 to 1989, he was the director of pulsed power laboratory at University of California, Irvine. From 1989 to 1999 he was a Senior Scientist at the Navy Research Laboratory in Washington DC. The fields he has worked on are relativstic electron beams, intense ion beams, Z-pinches, high power accelerators, and controlled fusion. Since then he is a visiting Scientist at the Israeli Institute of Technology and works on X-ray lasers, Z-pinches, and Q.I.P.